TÜBİTAK

Turkish Journal of Chemistry

http://journals.tubitak.gov.tr/chem/

Research Article

Turk J Chem
(2019) 43: 1503 – 1521

doi:10.3906/kim-1903-36

The solvatochromism and electronic structure of (E)-2-(2-hydroxystyryl)quinolin-8-ol

Ayşegül GÜMÜŞ[1,*], **Yadigar GÜLSEVEN SIDIR**[2], **İsa SIDIR**[2], **Selçuk GÜMÜŞ**[1]
[1]Department of Chemistry, Faculty of Science, Van Yüzüncü Yıl University, Van, Turkey
[2]Department of Physics, Faculty of Arts and Science, Bitlis Eren University, Bitlis, Turkey

Received: 12.03.2019 • **Accepted/Published Online:** 27.08.2019 • **Final Version:** 09.12.2019

Abstract: The (E)-2-(2-hydroxystyryl)quinolin-8-ol (abbreviated as HSQ) molecule was synthesized and characterized. The ESIPT, solvatochromism properties, electronic structure, and ground and excited electric dipole moments of this molecule were measured using absorption and fluorescence spectra recorded in 13 different solvents. Its electronic structure via electronic transitions was investigated to find the quantitative values of solvatochromism properties by LSER calculations. The ESIPT mechanism was clarified; ground and excited dipole moments were determined using solvatochromic shift methods. The DFT (B3LYP)/6-311++G(d,p) method and basis set with potential energy surface (PES) calculations of proton transfer were used to explain the ESIPT mechanism. NBO analysis, NLO properties, and behavior under an electric field were also determined.

Key words: 8-Hydroxyquinoline, 2-styrylquinoline, solvatochromism, electric dipole moment, electronic structure

1. Introduction

Quinoline derivatives have been used in many different applications such as optoelectronic materials and optical switches in nonlinear optics due to their unique electronic structure [1,2]. In addition, these compounds have some biological activities such as anticancer potential [1,3] and are used in the treatment of malaria, topical pathogenic parasitic *Leishmania* infection, antihepatitis B, etc. They have usage in textiles as well [4–6].

In particular, 8-hydroxyquinoline derivatives have attracted considerable interest due to their intramolecular proton transfer process properties. The physical and chemical effects of this challenging case in electronic structure are still being researched. Moreover, 8-hydroxyquinoline and its derivatives play an important role as chelating ligands for the preparation of various photo- and electroluminescent metal complexes [7,8] and fluorescent chemosensors for metal cations [9–16]. In addition, they exhibit strong pharmacological activities [17]. Naik et al., Filip et al., and Mehata et al. have investigated the electronic structure of 8-hydroxy quinoline and some of its derivatives [18–20].

Introduction of substituents, e.g., styryl groups, into the hydroxyquinoline ligand system enhances the thermal stability of metal complexes as compared to unsubstituted quinoline complexes and improves their solubility in organic solvents [21,22]. 2-Styrylquinoline derivatives are used as precursors for the synthesis of compounds exhibiting various biological activities, including antitumor [23], antifungal [24], antiinflammatory, and antiallergic [25]. In addition, they can be used as models for the design of molecular logic devices and supramolecular systems [26,27].

*Correspondence: gumusa@gmail.com

The traditional procedure for the synthesis of 2-styrylquinolines is based on condensation of quinaldine with aromatic aldehydes in acetic anhydride [28,29]. However, this method involves prolonged heating of the reaction mixture, while the yields of target compounds are reduced as a result of formation of products. In recent years, $Ca(OTf)_2$ catalyzed sp^3 C–H functionalization of azaarenes has been reported [30].

In the present study, we synthesized (E)-2-(2-hydroxystyryl)quinolin-8-ol (HSQ). Then we investigated its electronic structure, solvatochromism, electric dipole moment in the ground and excited state, and behavior under an electric field (EF). Knowledge of the interaction between solvent and solute and between solute and solute during electronic transitions and electronic structures of molecules provide important information on how electrons behave actively in photophysical and photochemical processes. Additionally, solvatochromism gives information involving the organic electronic material properties of molecules. It is worth noting that wavelength shifts (bathochromic and hypsochromic effect) occurring dependent on the solvent medium of electronic transitions can be explained by fitting to a quantitative model (polarity, dipolarity function, hydrogen bonding, or other physical parameters). The linear solvation energy relationship (LSER) was applied to analyze the solvent–solute interactions of the molecule. In order to achieve that, multilinear regression analysis (MLRA) was performed using Kamlet–Taft and Catalan parameters, the Marcus optical dielectric function, and Reichardt–Dimroth solvent parameters [31,32]. Excited state and ground state dipole moments of the investigated compounds were calculated using Bakhshiev, Lippert–Mataga, Bilot–Kawski, and Reichardt solvatochromic shift methods [32,33].

2. Experimental

2.1. General

All experiments were carried out in predried glassware in an inert atmosphere of argon. ^{1}H NMR and ^{13}C NMR spectra were recorded in $CDCl_3$ on an Agilent NMR spectrometer (400 MHz). ^{1}H (400 MHz) and ^{13}C NMR (100 MHz) were recorded in $CDCl_3$ and the chemical shifts are expressed in ppm relative to $CDCl_3$ (δ 7.26 and 77.0 for ^{1}H and ^{13}C NMR, respectively) as the internal standard. Flash column chromatography was performed using thick-walled glass columns and silica gel (60-mesh; Merck). The reactions were monitored by thin-layer chromatography (TLC) using Merck 0.2-mm silica gel 60 F254 analytical aluminum plates, visualized by UV light. All extracts were dried over anhydrous magnesium sulfate and solutions were concentrated under reduced pressure using a rotary evaporator.

Both absorbance and fluorescence spectra were recorded in cyclohexane, benzene, toluene, o-xylene, diethyl ether, chloroform, 1-butanol, acetone, ethanol, methanol, acetonitrile, ethylene glycol, and water. In these measurements, ultraviolet–visible (UV-Vis) absorption spectra and steady-state fluorescence spectra were recorded by PerkinElmer Lambda-35 UV-Vis spectrophotometer and PerkinElmer LS-55 Model fluorescence spectrophotometer. All the measurements were obtained at room temperature. The solutions were prepared as about 1.12 μM. Spectroscopic grade solvents and organic compounds were purchased from Sigma-Aldrich.

2.2. Synthesis and characterization

2-Methyl quinoline-8-ol (160 mg, 1 mmol), salicylaldehyde (122 mg, 1 mmol), $Ca(OTf)_2$ (5 mol %, 17 mg), and Bu_4NPF_6 (2 mol %, 8 mg) were mixed in a dark vial and reacted at 130 °C for 5 h. CH_2Cl_2 was added after the mixture was cooled. The crude product was purified by flash column chromatography using ethyl acetate/hexane as the eluent to give HSQ.

HSQ: Yellow solid. (80% yield; mp 190–192; ^{1}H NMR ($CDCl_3$, 400 MHz): δ 8.09 (d, J = 8.6 Hz, 1H), 8.01 (d, J = 16.4 Hz, 1H), 7.66 (t, J = 8.3 Hz, 2H), 7.43–7.37 (m, 2H), 7.28 (d, J = 8.2 Hz, 1H), 7.23–7.18 (m, 1H), 7.16 (dd, J = 1.1 and 7.5 Hz, 1H), 6.99 (t, J = 7.5 Hz, 1H), 6.84 (d, J = 8.0 Hz, 1H); ^{13}C NMR ($CDCl_3$, 100 MHz): δ 154.0, 153.8, 152.0, 137.9, 136.3, 129.8, 129.0, 127.8, 127.4, 127.2, 126.6, 123.7, 121.2, 120.4, 117.7, 116.1, 110.1. Characterization data are consistent with the literature data [34].

2.3. Experimental dipole moment calculations

Ground state electric dipole moments were calculated using the Bilot–Kawski method [35–41]. Excited state dipole moments were obtained by the Lippert–Mataga [42,43], Bakhshiev [44], and modified Bilot–Kawski methods [36,45] and the molecular-microscopic solvent polarity parameter (E_T^N) [46].

2.4. Quantitative solvent–solute interactions

LSER calculations of the title molecule were performed using Kamlet–Taft and Catalan parameters. These equations are shown below:

$$\vartheta_{max} = C_0 + C_1.f(n) + C_2.f(\varepsilon) + C_3.\beta + C_4.\alpha \quad (1)$$

$$\vartheta_{max} = C_5 + C_1.SP + C_2.SdP + C_3.SA + C_4.SB \quad (2)$$

In these equations, C_0 and C_5 are the statistical quantities corresponding to the values of these properties in the gas phase or inert solvents [47]. C_1–C_4 are coefficients derived from Kamlet–Taft solvatochromism, which provides information on solvent–solute interactions during electronic transitions. C_1 (polarizability or dispersion/polarization) and C_2 (polarity or orientation/induction) show specific interactions, while C_3 (hydrogen bonding acceptor) and C_4 (hydrogen bonding donor) show nonspecific interactions [48–50].

In Catalan solvatochromism, C_6 (polarizability of solvent) and C_7 (dipolarity of solvent) solvatochromic coefficients indicate the global interactions, while C_8 (solvent of acidity) and C_9 (solvent of basicity) describe the nonglobal interactions, which occur during electronic transitions between solvent and solute [51].

2.5. Quantum chemical calculations

The three-dimensional ground state (S_0) geometries of all compounds were optimized in the gas phase without any symmetry restrictions using DFT [52] implemented hybrid functional B3LYP with the Gaussian 09W [53] software package. B3LYP is composed of Becke's three parameter exchange functional (B3) [54] and the nonlocal correlation functional by Lee, Yang, and Parr (LYP) [55]. In order to find the molecular structures with minimum energy, conformational analysis was performed with the B3LYP/6-311++G(d,p) method and basis set. Afterwards, H-bond transfer of O28–H21 with N10–H21 was performed by applying the TD-B3LYP/6-311++G(d,p) method and basis set. The vibrational analyses were carried out using the same basis set employed in the corresponding geometry optimizations. The frequency analysis did not yield any imaginary frequencies, indicating that the optimized structure of the molecule corresponds to at least a local minimum on the potential energy surface. The normal mode analysis was performed for 3N – 6 vibrational degrees of freedom, with N being the number of atoms in the molecule.

3. Results and discussion

Through the cleavage of two C(sp^3)–H bonds of alkylazaarenes, synthesis of alkenyl product by green Lewis acid catalyst was considered. The HSQ was synthesized by the reaction of 2-methyl quinoline-8-ol and salicylaldehyde by the catalysis of $Ca(OTf)_2$ (Scheme).

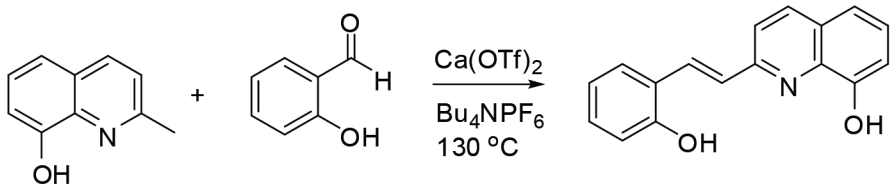

Scheme 1. Synthesis of HSQ.

3.1. Electronic transitions

Figure 1 depicts the molecular structure including the Mulliken charge and dipole moment vectors calculated using B3LYP/6-311++G(d,p) of HSQ.

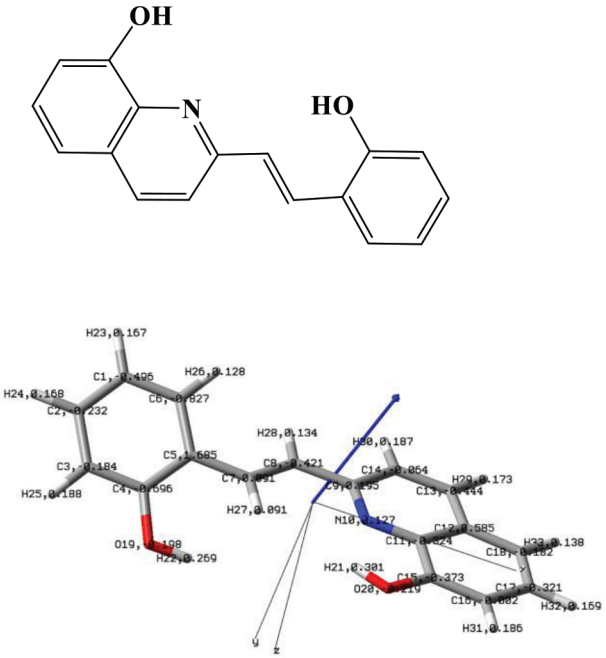

Figure 1. Molecular structure, Mulliken charge, and dipole moment vectors of the HSQ molecule calculated using B3LYP/6-311++G(d,p).

Table 1 and Figure 2 show the absorbance and fluorescence spectra data of the HSQ molecule in various solvent media. We observed that the absorption spectrum of this molecule has four absorption bands in 13 different solvents. These electronic bands are observed at 248–256 nm (5.00–4.84 eV), 260–285 nm (4.77–4.35 eV), 293–311 nm (4.23–3.99 eV), and 344–361 nm (3.60–3.43 eV), respectively. The first electronic absorbance transition peak observed in the absorbance spectrum can be referred to as $\pi-\pi^*$ electronic transition, which was observed in cyclohexane, diethyl ether, methanol, acetonitrile, ethylene glycol, and water. Except for cyclohexane and diethyl ether, all of these solvents are polar protic, which may have an effect on electronic transitions. However, in cyclohexane, only intramolecular electronic transitions can take place. The second

electronic band can be attributed to $\pi-\pi^*$ electronic absorption in the quinoline ring, while the first electronic band is attributed to $\pi-\pi^*$ electronic absorption transition in the phenol ring. The third electronic band occurred by $\pi-\pi^*$ electronic absorption transition due to conjugation between the quinoline and phenol rings. The last band refers to n–π^* electronic absorption transition, which is expected to be born out from the delocalization of n electrons as a result of the interaction of HSQ with solvents. The assignment of the absorption bands is made according to the transition energy (in eV) and the electron conjugation centers of the molecule. Naik and Math reported that the 8-hydroxyquinoline molecule has an excited state intramolecular proton transfer (ESIPT) mechanism [18]. Filip et al. investigated the electronic structure of the 8-hydroxyquinoline molecule in some solvents and thus an ESIPT structure has been explained for this molecule [19]. Electronic structure and dipole moments estimated by using polar and aprotic solvents the 2-,6-,7-, 8-hydroxyquinolines were researched by Mehata et al. [20]. The observed electronic transition wavelength values for both absorption and emission spectra in these works were smaller than those in the present work, because the phenoxy substituent gives rise to longer wavelengths. Greater wavelength values brought about a fine structure in the spectra of HSQ.

Table 1. The absorbance and fluorescence spectra data of HSQ.

Solvent	λ_{abs1}	λ_{abs2}	λ_{abs3}	λ_{abs4}	ν_{abs4}	λ_{pl1}	λ_{pl2}	ν_{pl2}	λ_{pl3}	$\Delta\nu$
Cyclohexane	256	-	-	349	28,653	408	441	22,675	-	5977
Benzene	-	287	296, 311	346	28,901	415	435	22,988	510	5913
Toluene	-	-	-	344	29,069	411	445	22,471	515	6597
o-Xylene	-	-	-	346	28,901	414	438	22,831	-	6070
Diethyl ether	249	285	295	350	28,571	-	428	23,364	-	5206
Chloroform	-	286	296	347	28,818	418	436	22,935	-	5882
1-Butanol	-	286	295, 311	354	28,248	-	441	22,675	-	5572
Acetone	-	-	-	352	28,409	-	439	22,779	-	5630
Ethanol	-	285	295	350	28,571	-	446	22,421	480	6149
Methanol	248	285	294	350	28,571	-	454	22,026	482	6544
Acetonitrile	249	285	293	351	28,490	-	444	22,522	478	5967
Ethylene glycol	251, 264	-	298	361	27,700	416	446	22,421	-	5279
Water	260	-	-	355	28,735		446	22,421	-	6314

In the first three absorbance bands, there occurred an irregular hypsochromic shift in which the bands shifted towards smaller wavelengths with increasing polarity. During these electronic transitions, the molecule decreased the difference between ground and excited state energies dependent on the polarity of the solvent.

As the polarity increases, the wavelength of the last absorbance band shifts towards a higher value, which indicates a bathochromic shift. This electronic transition might be a result of excited state intramolecular proton transfer. The energy of this transition is increased as the polarity increases. As can be seen from Table 1, Stokes shifts vary in the range of 78–101 nm (5206–6597 cm^{-1}). This means that the studied molecule proves excited state intramolecular proton transfer. The fine structure observed in the fluorescence spectra supports an ESIPT mechanism too. The values of fluorescence bands are shown in Table 1. Three fluorescence bands were observed for the present molecule. The wavelength of the excitation was 360 nm. The first fluorescence band was at 408–418 nm (3.04–2.97 eV). The second fluorescence band was observed in all solvents at 428–454 nm

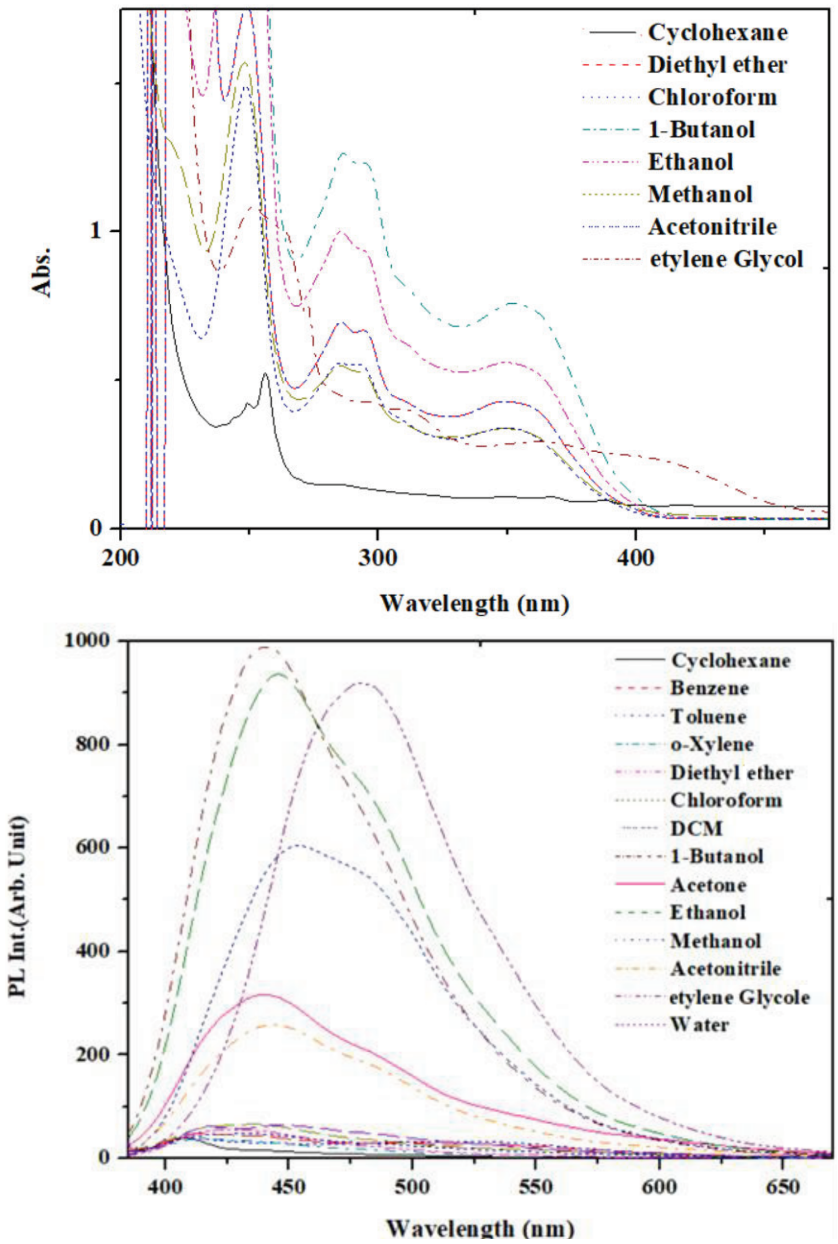

Figure 2. The absorbance and fluorescence spectra data in different solvent media of HSQ (excitation wavelength is 360 nm).

(2.90–2.73 eV). The last fluorescence band appeared in several solvents (benzene, toluene, ethanol, methanol, and acetonitrile) in the range of 478 nm (2.59 eV) and 515 nm (2.41 eV). In both the first and the second fluorescence bands, a bathochromic shift was observed irregularly due to the solvent polarity change. The hypsochromic shift in the third fluorescence band was observed irregularly.

Stokes shifts between the electronic absorbance and fluorescence bands studied have a bathochromic effect, indicating solvatochromism. Figure 3 shows the open and closed forms of the present structure (Figure 3a), geometry optimized structures of open and closed forms (Figure 3b), and excited state intramolecular proton transfer mechanism of the molecule (Figure 3c) studied by B3LYP/6-311++G (d,p) level of theory. As

seen from Figure 3a, the distance between 21 H with 10 N was 2.1048 Å, which means that this proton can form hydrogen bonding with the nitrogen atom in the excited state.

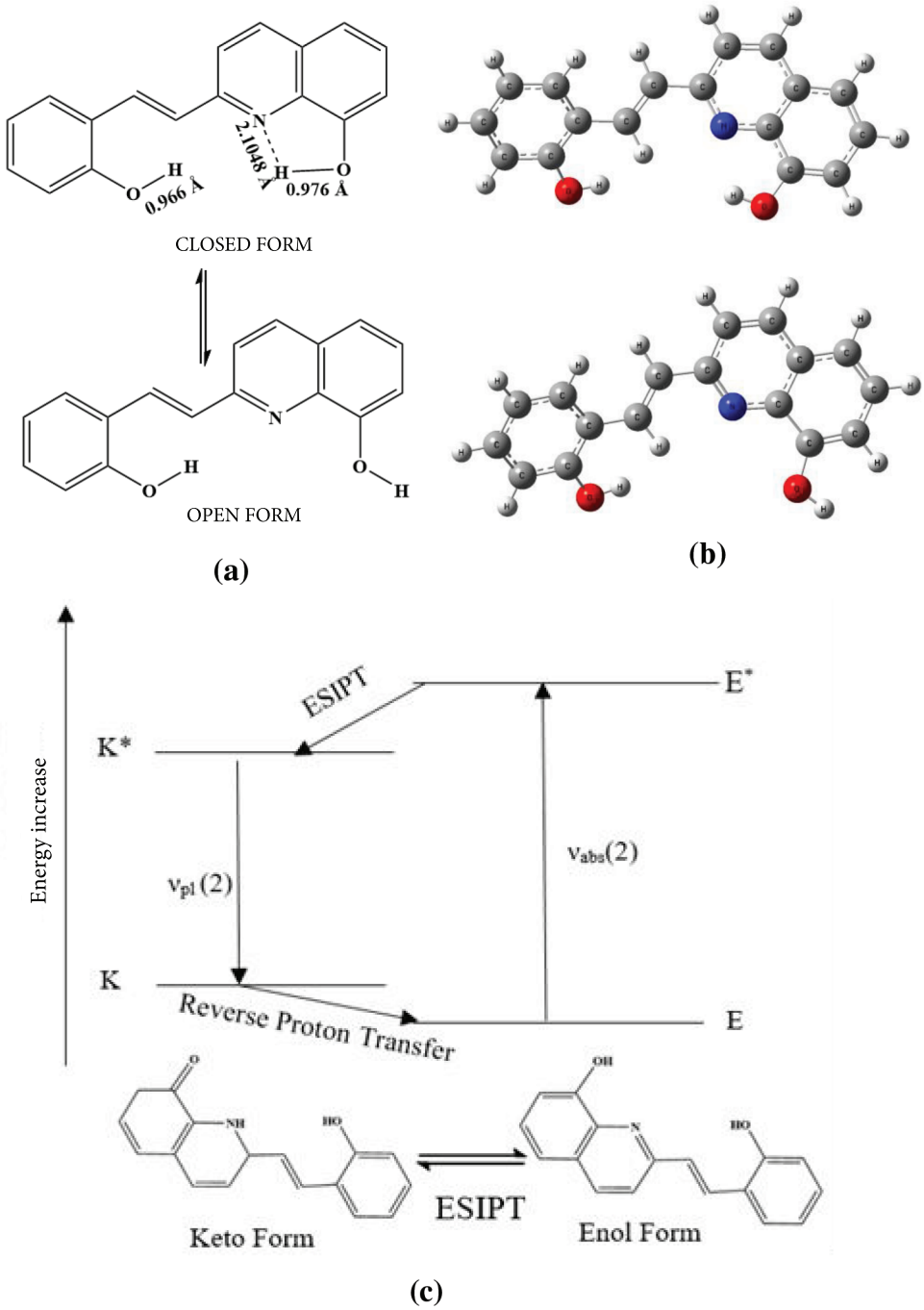

Figure 3. Excited state intramolecular proton transfer mechanism of the molecule calculated with B3LYP/6-311++G(d,p) for HSQ.

3.2. Solvatochromism

Solvatochromism is the reversible change in the electronic spectroscopic properties (absorption, emission) of a chemical structure caused by solvents. In other words, the term solvatochromism is used to describe significant changes in the position (and sometimes intensity) of the UV-Vis absorption band accompanying the change in the polarity of the medium. Molecules of electronic transitions depending on the environment can be used in organic electronics [46,47].

The linear solvation energy relationship allows us to statistically identify the effects that contribute to solvatochromism, quantitatively and qualitatively defining the interactions between solvent and solute. The studied molecule was subjected to LSER for both absorbance and fluorescence using dielectric function and refractive index Kamlet–Taft parameters. In addition, LSER was applied using solvent polarizability, solvent dipolarity, solvent of acidity, and solvent of basicity done with Catalan parameters. The resulting statistical parameters for correcting the multiple linear regression equations and the proposed models are given below. The values of parameters used in the solvatochromism and electric dipole moment calculations are tabulated in Table 2.

Table 2. Spectral treatment of the Bilot–Kawski, Lippert–Mataga, Bakhshiev, modified Bilot–Kawski, and Reichardt methods.

Methods	Slope (m)	Intercept	Cor. (R^2)	Solvents used	n
Bilot–Kawski-1	1753.8	4441.8	0.7788	Diethyl ether, 1-Butanol, Acetone, Acetonitrile, Water	5
Bilot–Kawski-2	–1805.2	53,455	0.8895	Diethyl ether, 1-Butanol, Acetone, Acetonitrile, Water	5
Lippert–Mataga	1429	5981.6	0.8711	Cyclohexane, Benzene, o-Xylene, Methanol, Water	5
Bakshiev	502.63	5984.1	0.8544	Cyclohexane, Benzene, o-Xylene, Methanol, Water	5
Modified Bilot–Kawski	–1608.1	26,595	0.8987	Benzene, Diethyl ether, Chloroform, 1-Butanol, Acetone, Ethanol, Acetonitrile, Water	8
Reichardt	1742.6	5139.8	0.8614	Diethyl ether, Chloroform, Acetone, Ethanol, Methanol, Acetonitrile	6

Eqs. (3) and (4) are the equations of Kamlet–Taft and Catalan solvatochromism for the fourth absorbance electronic transition. Ethylene glycol was removed to make the necessary numerical statistical parameters (for R, R^2, F, and P) in both Kamlet–Taft and Catalan solvatochromism. For the studied molecule, C_0 data were obtained as 27,773 cm^{-1} (360 nm) and 28,343 cm^{-1} (352 nm) from the Kamlet–Taft and Catalan models, respectively. These values are determined for the molecule without any interaction with the environment. In both Kamlet–Taft and Catalan solvatochromism, the polarizability in specific interactions is observed to be more effective, so that as the polarity (dispersion/polarization) increases the wavelength shifts to smaller values, i.e. the hypsochromic shift occurs with increasing polarity. Although the polarity parameter is not dominant in the electronic absorbance transitions, a bathochromic shift is observed with increasing polarity (dipolarity-orientation). According to Eq. (3), the hydrogen bond acceptor is more effective than the donor in electron absorption transitions. According to Eq. (4), the solvent of basicity was observed to be more dominant

than the solvent of acidity.

$$\vartheta_{max} = 28343 + 2146.f(n) - 144.f(\varepsilon) - 494.\beta + 158.\alpha \quad (3)$$

$$R = 0.856R^2 = 0.733F = 4.796P = 0.035n = 12 \text{ extracting ethylene glycol}$$

$$\vartheta_{max} = 27773 + 1531.SP - 155.SdP + 115.SA - 334.SB \quad (4)$$

$$R = 0.866R^2 = 0.749F = 5.235P = 0.029n = 12 \text{ extracting ethylene glycol}$$

For the electronic emission spectrum, Kamlet–Taft solvatochromism and Catalan solvatochromism were applied extracting cyclohexane, benzene, chloroform, and methanol. In Eqs. (5) and (6), C_0 and C_5 coefficients in Kamlet–Taft and Catalan solvatochromism of HSQ were 25,644 cm^{-1} (389 nm) and 21,040 cm^{-1} (475 nm), respectively. These wavelengths are electronic emission transition wavelengths in gaseous/inert medium. According to the Kamlet–Taft solvatochromism, the polarization/dispersion effect is influenced by the orientation/induction effect.

In Eq. (5), the electronic emission wavelength shifts toward a greater value by increasing polarization/dispersion and orientation/induction function; this indicates the bathochromic effect. Looking at the specific interactions, the hydrogen bond donor has a greater effect than the hydrogen bond acceptor does. The hydrogen bond acceptor effect causes the hypsochromic effect. According to Eq. (6), solvent dipolarity has a greater effect on electronic emission transition than solvent polarizability does. According to the solvent polarity, it seems that there is a bathochromic effect in electronic emission transitions. Comparing the solvent basicity, solvent acidity has a more significant effect on the spectral shift. Both solvent acidity and solvent basicity give rise to a bathochromic effect on the electronic emission band.

$$\vartheta_{max} = 25644 - 8684.f(n) - 1450.f(\varepsilon) + 525.\beta - 192.\alpha \quad (5)$$

$$R = 0.866R^2 = 0.750F = 3.000P = 0.156n = 9 \text{ extracting cyclohexane, benzene, chloroform, methanol}$$

$$\vartheta_{max} = 21040 + 2192.SP + 46.SdP - 914.SA - 470.SB \quad (6)$$

$$R = 0.840R^2 = 0.706F = 3.599P = 0.079n = 12 \text{ extracting diethyl ether, water}$$

3.3. Electric dipole moments

The ground and excited state dipole moments were estimated using solvatochromic shift methods. The ground state dipole moment was calculated using the Bilot–Kawski method, while the excited state dipole moment of HSQ was calculated using the Bilot–Kawski, Lippert–Mataga, Bakshiev, modified Bilot–Kawski, and Reichardt methods. Figure 4 depicts the correlation plots derived from the Bilot–Kawski, Lippert–Mataga, Bakshiev, modified Bilot–Kawski, and Reichardt methods. These calculations were used to obtain Stokes shifts and the sum of wavenumbers of the fluorescence and absorbance spectra. In addition, these calculations were used to find dielectric and refraction index functions and Onsager cavity radius. Moreover, the statistical parameters found in the experimental dipole moment calculations are listed in Table 3. The ground state dipole moment was 0.0886 D by the Bilot–Kawski method, whereas the excited state dipole moment was 6.09 D, 5.546 D, 3.325 D, 5.791 D, and 3.394 D with the Bilot–Kawski, Lippert–Mataga, Bakshiev, modified Bilot–Kawski, and Reichardt methods, respectively. In addition, Onsager cavity radius and electric dipole moment values are given in Table 4. The ground state and excited state dipole moments of the 8-hydroxy quinoline were reported as 0.87 D and

2.02 D, respectively [20]. The ground state dipole moment of HSQ with hydroxystyryl substituent decreases, while its excited state dipole moment increases. This case is attributed to the breaking of conjugation between the quinoline ring and hydroxystyryl substituent. A decrease in the excited state charge distribution compared to the ground state of charge distribution was observed. There is a considerable difference between the ground and the excited state dipole moments. Thus, in the excited state, large changes in electronic construction occurred.

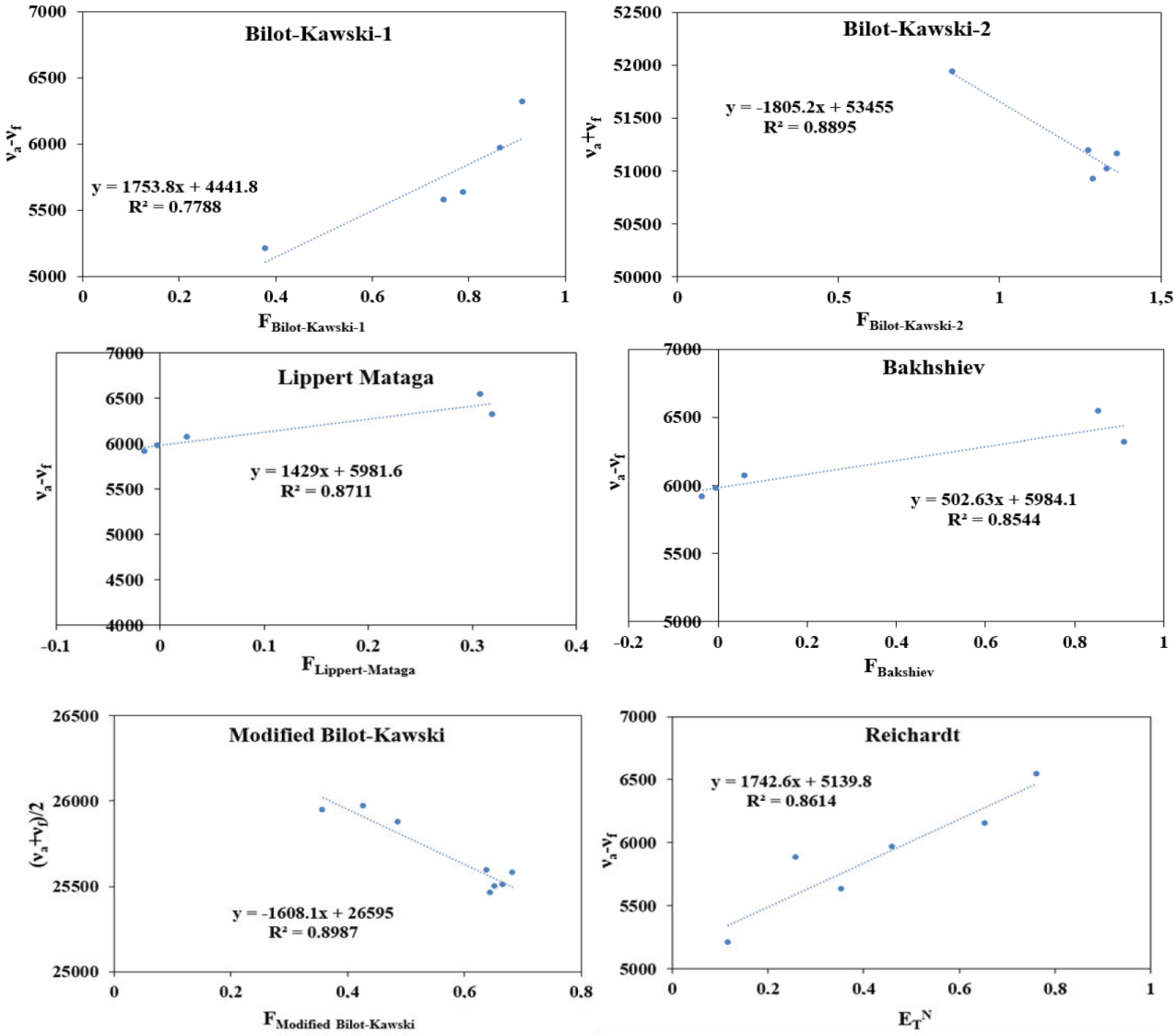

Figure 4. The graphs of electric dipole moment correlations.

3.4. ESIPT reaction

Proton transfer consisting of the O–H...N group in this molecule was explored by calculating both the ground and excited state geometries using the B3LYP/6-311++G(d,p) and TD-B3LYP/6-311++G(d,p) methods and potential energy surface (PES) curves. The plot of PES depending on proton migration from the O_{20}–H_{21}

Table 3. Onsager cavity radius and electric dipole moments.

Methods	Dipole moment (Debye)
μ_g (Bilot–Kawski)	0.0886
μ_e (Bilot–Kawski)	6.09
μ_e (Lippert–Mataga)	5.546
μ_e (Bakshiev)	3.325
μ_e (Modified Bilot–Kawski)	5.791
μ_e (Reichardt)	3.394
$\mu_{theo.}$	3.3811
a	5.93 Å

Table 4. The values of parameters used in solvatochromism and electric dipole moment calculations.*

No.	Solvent	ε	n	β	α	f(ε)	f(n)	SP	SdP	SA	SB
1	Cyclohexane	2.02	1.4266	0	0	0.2537	0.2565	0.683	0.000	0.000	0.073
2	Benzene	2.27	1.5589	0.1	0	0.2974	0.3228	0.793	0.270	0.000	0.124
3	Toluene	2.38	1.4969	0.11	0	0.3151	0.2925	0.791	0.266	0.000	0.157
4	o-Xylene	2.57	1.5054	0.16	0	0.3435	0.2968	0.782	0.284	0.000	0.128
5	Diethyl ether	4.34	1.3497	0.47	0	0.5268	0.2150	0.617	0.385	0.000	0.562
6	Chloroform	4.81	1.4459	0.1	0.2	0.5595	0.2666	0.783	0.614	0.047	0.071
7	1-Butanol	17.4	1.399	0.84	0.84	0.8454	0.2418	0.674	0.655	0.341	0.809
8	Acetone	20.56	1.3587	0.48	0.08	0.8670	0.2199	0.651	0.907	0.000	0.475
9	Ethanol	24.55	1.3614	0.75	0.86	0.8870	0.2214	0.633	0.783	0.400	0.658
10	Methanol	32.66	1.3284	0.66	0.98	0.9134	0.2031	0.608	0.904	0.605	0.545
11	Acetonitrile	38.8	1.3442	0.4	0.19	0.9265	0.2119	0.645	0.974	0.044	0.286
12	Ethylene glycol	41.4	1.4318	0.86	0.75	0.9309	0.2592	0.777	0.910	0.717	0.534
13	Water	78.36	1.333	0.18	1.17	0.9627	0.2056	0.681	0.997	1.062	0.025

Experimental values of solvent parameters dielectric constant ε, refractive indices n, Reichardt parameter (ETN) [29,30], Kamlet–Taft parameters (solvent dipolarity/polarizability parameter, π, H-bonding donor capacity α, H-bonding acceptor capacity β), Catalan parameters (solvent polarity SP, solvent dipolarity SdP, acidity of solvent SA, basicity of solvent SB) are taken from the literature [29–35].

group toward the N atom is depicted in Figure 3c. In addition, we saw the proton transfer in the PES video. In the ground state, O20–H21 length is 0.97438 Å, while H21…N10 bond length is 2.09721 Å. In the excited state, O20–H21 bond length in the ESIPT mechanism is calculated to be 2.35779 Å, whereas H21…N10 bond length is found to be 0.99721 Å. The energy difference between these two states in ground state is 0.6684 eV, while in excited state it is 0.5910 eV. It can be concluded from Figure 5 that the third absorbance, the second photoluminescence, and the fourth absorbance of the molecule occur in the closed form of the molecule, while the second fluorescence occurs by the electronic transition of the ESIPT mechanism.

In cyclohexane, we have two electronic absorption transition and two fluorescence bonds. The ESIPT mechanism was observed at the fourth electronic absorbance transition. According to Figure 5, the O–H bond

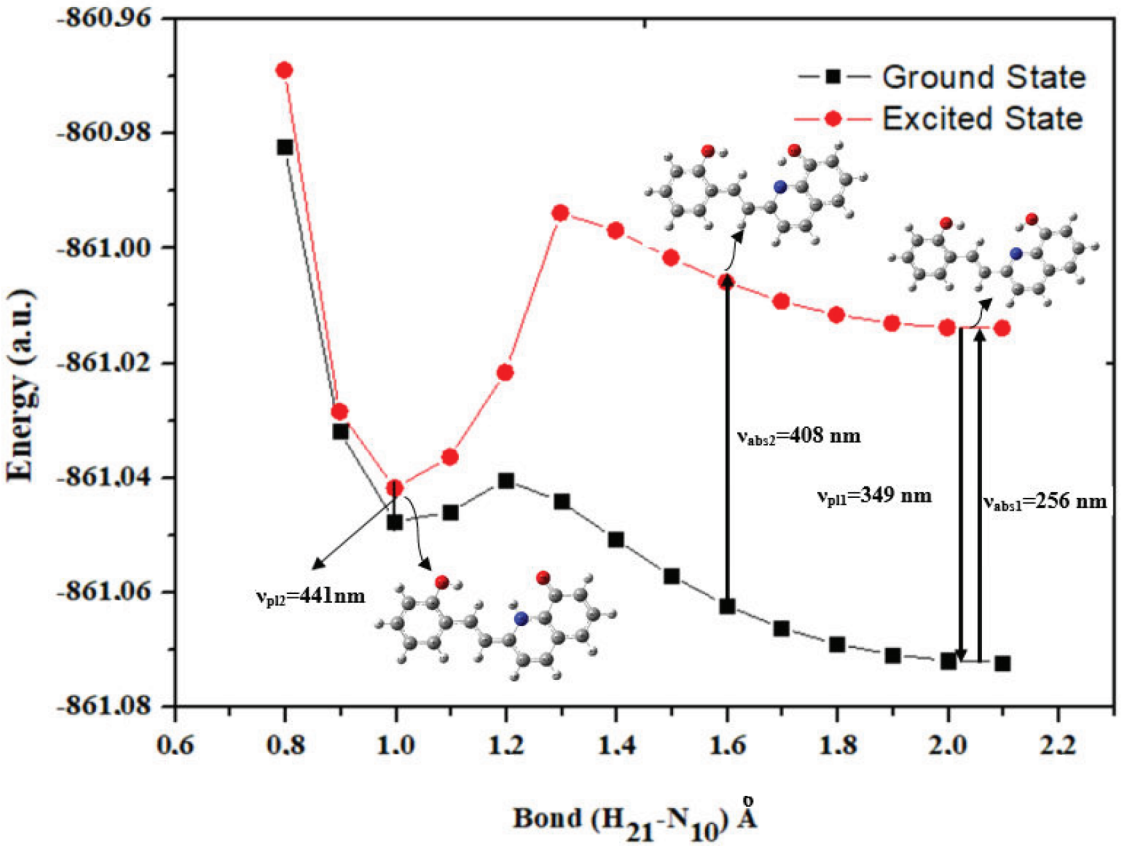

Figure 5. ESIPT mechanism calculated with B3LYP/6-311++G(d,p) and TD-B3LYP/6-311++G(d,p) for H-transfer of HSQ. Electronic transition mechanism in benzene is presented.

is broken in the course of the second electronic transition. Therefore, H migrates from H–O to the N_{10} atom. Figure 3c shows the ESIPT mechanism of HSQ [56].

3.5. Treatment under an Electric Field

HOMO and LUMO energies and the HOMO–LUMO gap ($\Delta\varepsilon$) of HSQ calculated by DFT-B3LYP/6-311++G(d,p) level of theory were –5.89 eV, –2.40 eV, and 3.49 eV, respectively. A large $\Delta\varepsilon$ value in the ground state indicates that HSQ is an insulator. The ground state dipole moment of the present compound was calculated as 3.3684 Debye by the same method. In order to tune the $\Delta\varepsilon$ and dipole moment, an external EF was applied in 3D (xyz-direction). The plots of $\Delta\varepsilon$ variation and dipole moment change versus applied external EF are depicted in Figures 6 and 7, respectively. As seen from Figure 6, $\Delta\varepsilon$ stays almost stable up to 0.04 V/Å EF. From 0.05 V/Å to 0.08 V/Å, $\Delta\varepsilon$ decreases drastically from 3.0330 eV to 0.8702 eV. At the higher applied EF, the decrease in $\Delta\varepsilon$ continues and the smallest $\Delta\varepsilon$ value is obtained at 0.17 V/Å as 0.3951 eV. It is important to note that at 0.07 V/Å EF and beyond HSQ gains an organic semiconductor character. LUMO energy starts to decrease under 0.05 V/Å EF, whereas the response of HOMO energies versus EF starts at 0.08 V/Å. The external EF was more effective on LUMO energy than on HOMO energy.

Dipole moment of the title compound was calculated to be 3.3684 Debye in the absence of EF by DFT-B3LYP/6-311++G(d,p) level of theory. In the range of 0.00–0.06 V/Å EF, dipole moment was 3.368–3.6786

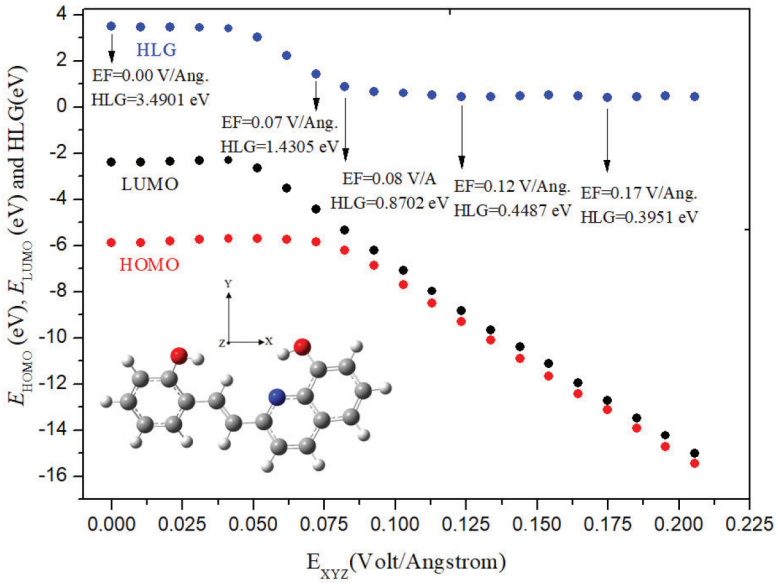

Figure 6. HOMO and LUMO energies and HOMO–LUMO gap ($\Delta\varepsilon$) as a function of external electric field.

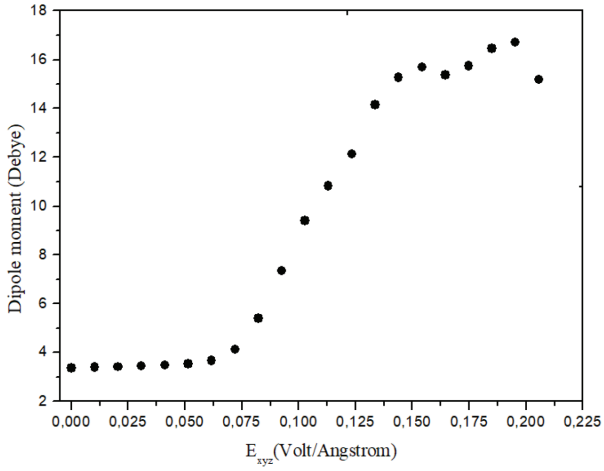

Figure 7. Dipole moment variation versus external electric field.

Debye. Starting from the 0.07 V/Å EF, dipole moment increased almost linearly until 0.15 V/Å. At higher EF beyond this point dipole moment showed fluctuations. The highest dipole moment was 16.7037 Debye at 0.19 V/Å EF.

3.6. Nonlinear optical (NLO) properties

NLO effects emerge from the interactions of electromagnetic fields in various media to generate new fields changed in phase, frequency, amplitude, or other diffusion characteristics from the incident fields [57]. NLO materials have been widely investigated by researchers recently due to their importance in applicability as the key functions of frequency shifting, optical logic, optical switching, optical modulation, and optical memory for the upcoming technologies in areas of telecommunications, signaling and optical interconnections [58–61].

A Taylor series expansion of the total dipole moment, μ_{tot} (Eq. (7)), induced by the field represents the

NLO response of an isolated molecule in an EF $E_i(\omega)$:

$$\mu_{tot} = \mu_0 + \alpha_{ij}E_j + \beta_{ijk}E_{jk}, \tag{7}$$

where α, μ_0, and β_{ijk} are linear polarizability, the permanent dipole moment, and the first hyperpolarizability tensor, respectively. The isotropic (or average) linear polarizability can be calculated by Eq. (9) [62]:

$$\alpha_{tot} = (\alpha_{xx} + \alpha_{yy} + \alpha_{zz})/3 \tag{8}$$

First hyperpolarizability is a third degree tensor that is represented by a 3 × 3 × 3 matrix. The 27 elements of the 3D matrix can be reduced to 10 components due to the Kleinman symmetry [62] such that $\beta_{xyy} = \beta_{yxy} = \beta_{yyx} = \beta_{yyz} = \beta_{yzy} = \beta_{zyy}$; ...). The output file of a computation in Gaussian 09 provides the 10 values of this matrix as β_{xxx}, β_{xxy}, β_{xyy}, β_{yyy}, β_{xxz}, β_{xyz}, β_{yyz}, β_{xzz}, β_{yzz}, and β_{zzz}, respectively. The components of the first hyperpolarizability can be calculated using the following equation (Eq. (9)) [63]:

$$\beta_i = \beta_{iii} + 1/3?(\beta_{ijj} + \beta_{jij} + \beta_{jji}) \tag{9}$$

The magnitude of β_{tot} from Gaussian program output can be calculated by Eq. (10).

$$\beta_{tot} = [(\beta_{xxx} + \beta_{xyy} + \beta_{xzz})^2 + (\beta_{yyy} + \beta_{yzz} + \beta_{yxx})^2 + (\beta_{zzz} + \beta_{zxx} + \beta_{zyy})^2]^{1/2} \tag{10}$$

The calculations of the total molecular dipole moment (μ_{tot}), linear polarizability (α_{tot}), and hyperpolarizability (β_{tot}) from the Gaussian output were explained in a previous work [64], and DFT has been widely used as an effective method to compute the properties of NLO materials [65]. The electronic dipole moment μ_{tot}, polarizability α_{tot}, and the hyperpolarizability β_{tot} data of all compounds were calculated at the B3LYP/6-311++G(d,p) level of theory using the Gaussian 09 package; the results are given in Table 5.

Table 5. The B3LYP/6-311++G(d,p) calculated dipole moment μ_{tot} (Debye), the average polarizability α_{tot} (Å^3), and first hyperpolarizability β_{tot} ($\times 10^{-30}$ cm^5/esu) for HSQ.

μ_x	0.5383	β_{xxx}	2139.504961
μ_y	–3.3117	β_{xxy}	–512.403
μ_z	0.4183	β_{xyy}	–95.3790815
μ_{tot}	3.3811	β_{yyy}	–293.6318287
α_{xx}	269.679	β_{xxz}	65.8297021
α_{xy}	7.995	β_{xyz}	13.1822671
α_{yy}	204.118	β_{yyz}	–3.5988129
α_{xz}	–15.755	β_{xzz}	–7.101
α_{yz}	0.707	β_{yzz}	–77.1840884
α_{zz}	151.831	β_{zzz}	–31.5506389
α_{tot}	38.0	β_{tot}	19.2

The dipole moment of HSQ was calculated to be 3.37 Debye. Two hydroxyl groups attached to parent quinoline result in an increase in charge separation; thus, the observation of high dipole moment is not surprising.

The 3D-MEP surface counter map was obtained for B3LYP/6-311++G(d,p) optimized geometries to predict reactive sites for electrophilic and nucleophilic processes for the compounds and dipole moment observation. The electrostatic potential surface of HSQ is shown in Figure 8. Electrophilic reactivity regions (negative charge) are shown in red and yellow, while blue indicates nucleophilic reactivity [66]. For the title compound, the negative charge is mostly localized on the electron withdrawing hydroxy groups, as expected. The charge separation is very well observed for HSQ, which may be the reason for the high magnitude dipole moment.

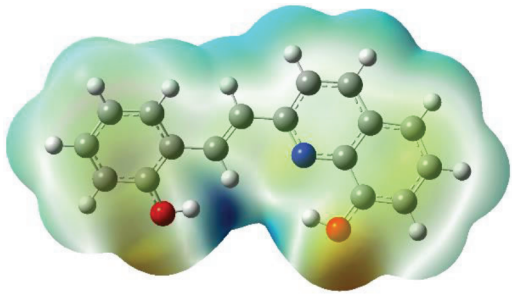

Figure 8. MEP for the title compound calculated by B3LYP/6-311++G(d,p).

The average polarizability (α_{tot}) data together with its components are listed in Table 5. The value of the calculated polarizability is equal to 38.0 Å^3 for HSQ. The hyperpolarizability value β_{tot} (19.2 $\times$ 10^{-30} cm^5/esu) for the compound was much greater than that of urea (0.77 $\times$ 10^{-30} cm^5/esu) [67], which is one of the typical compounds used in research into the NLO properties of molecular systems. Therefore, it was used frequently as a threshold value for comparative studies [67]. The obtained results show that the title compound is a good candidate for NLO materials. The hyperpolarizability value for hydroxyquinoline itself was computed to be 3.5; thus, an increase in the conjugation path upon substitution of the hydroxystyryl link resulted in an increase in first hyperpolarizability. Comparison of the interfrontier energy gap data with the hyperpolarizability values is a good indicator of nonlinear properties. ΔE for urea was calculated to be 8.2 eV at the same level of DFT method, whereas the ΔE value for the present system was 3.49 eV.

4. Conclusions

In the present study, the electronic structure, ESIPT mechanism, experimental dipole moment, and solvatochromism properties of HSQ were investigated by both spectroscopic and computational methods. HSQ was found to be a solvatochromic material. Global electronic absorption and emission transitions indicated a bathochromic effect. Charge distribution in ground and excited states was almost the same, due to μ_e being only 0.0144 times bigger than μ_g. The equation $\mu_e = (\mathrm{m}_{B-K(2)} + \mathrm{m}_{B-K(1)})/(\mathrm{m}_{B-K(2)} - \mathrm{m}_{B-K(1)})$ was used to obtain the charge distribution data [35–40]. It was observed that application of an external EF gave rise to a lower value of $\Delta\varepsilon$ and thus gave an organic semiconductor character of HSQ. The lowest HOMO–LUMO band gap was obtained at 0.17 V/Å as 0.3951 eV.

Acknowledgments

We are grateful to the Presidency of Scientific Research Projects of Van Yüzüncü Yıl University for its financial support (2015-FEN-B326). The authors greatly acknowledge the support of Bitlis Eren University Scientific and Technological Application and Research Center.

References

1. Afzal O, Kumar S, Haider MR, Ali MR, Kumar R et al. A review on anticancer potential of bioactive heterocycle quinoline. European Journal of Medicinal Chemistry 2015; 97: 871-910.
2. El-Ghamaz NA, El-Menyawy EM, Diab MA, El-Bindary AA, El-Sonbati AZ et al. Optical and dielectrical properties of azo quinoline thin films. Solid State Sciences 2014; 30: 44-54.
3. Gayathri K, Radhika R, Shankar R, Malathi M, Savithiri K et al. Comparative theoretical and experimental study on novel tri-quinoline system and its anticancer studies. Journal of Molecular Structure 2017; 1134: 770-780.
4. Luongo G, Iadaresta F, Moccia E, Östman C, Crescenzi C. Determination of aniline and quinoline compounds in textiles. Journal of Chromatography A 2016; 1471: 11-18.
5. Kaur M, Jain M, Reddy RP, Jain R. Quinolines and structurally related heterocycles as antimalarials. European Journal of Medicinal Chemistry 2010; 45: 3245-3264.
6. Kidwai M, Bhushan KR, Sapra P, Saxena RK, Gupta R. Alumina-supported synthesis of antibacterial quinolines using microwaves. Bioorganic & Medicinal Chemistry 2000; 8: 69-72.
7. Hunga LS, Chen CH. Recent progress of molecular organic electroluminescent materials and devices. Materials Science and Engineering: R: Reports 2002; 39: 143-222.
8. Chen CH, Shi J. Metal chelates as emitting materials for organic electroluminescence. Coordination Chemistry Reviews 1998; 171: 161-174.
9. Song KCh, Kim JS, Park SM, Chung KC, Ahn S et al. Fluorogenic Hg^{2+}-selective chemodosimeter derived from 8-hydroxyquinoline. Organic Letters 2006; 8: 3413-3416.
10. Zhang H, Wang QL, Jiang YB. 8-Methoxyquinoline based turn-on metal fluoroionophores. Tetrahedron Letters 2007; 48: 3959-3962.
11. Li Z, Xi P, Huang I, Xie G, Shie Y et al. A highly selective fluorescent chemosensor for Cd(II) based on 8-hydroxyquinoline platform. Inorganic Chemistry Communications 2011; 14: 1241-1244.
12. Zhu H, Fan J, Lu J, Hu M, Peng X. Optical Cu^{2+} probe bearing an 8-hydroxyquinoline subunit: high sensitivity and large fluorescence enhancement. Talanta 2012; 93: 55-61.
13. Haggag SMS, Farag AAM, Abdelrafea M. Spectral, thermal and optical–electrical properties of the layer-by-layer deposited thin film of nano Zn(II)-8-hydroxy-5-nitrosoquinolate complex. Spectrochimica Acta Part A: Molecular and Biomolecular Spectroscopy 2013; 110: 14-19.
14. Ouyang X, Wang G, Zeng H, Zhang W, Li J. Design and synthesis of 2-substituted-8-hydroxyquinline zinc complexes with hole-transporting ability for highly effective yellow-light emitters. Journal of Organometallic Chemistry 2009; 694: 3511-3517.
15. Shabestary N, Ashraf M, Bayoumi EL. A unique excitation wavelength dependence of excited-state proton transfer in para-N,N-dimethylaminosalicylic acid. Chemical Physics Letters 1984; 106: 102-110.
16. Issa TB, Hassine CBA, Ghalla H, Barhoumi H, Benhamada L. Experimental and computational study of electronic, electrochemical and thermal properties of quinoline phosphate. Journal of Molecular Structure 2018; 1162: 71-80.
17. Zouhiri F, Mouscadet JF, Mekouar K, Desmaële D, Savouŕe D et al. Structure-activity relationships and binding mode of styrylquinolines as potent inhibitors of HIV-1 integrase and replication of HIV-1 in cell culture. Journal of Medicinal Chemistry 2000; 43: 1533-1540.
18. Naik LR, Math NN. Photo physical properties of 8-hydroxy quinoline. Indian Journal of Pure and Applied Physics 2005; 43: 743-749.
19. Filip EM, Humelnicu IV, Ghirvu CI. Some aspects of 8-hydroxyquinoline in solvents. Acta Chemica IASI 2009; 17: 85-96.

20. Mehata MS, Singh AK, Sinha RK. Experimental and theoretical study of hydroxyquinolines: hydroxyl group position dependent dipole moment and charge-separation in the photoexcited state leading to fluorescence. Methods and Applications in Fluorescence 2016; 4: 045004-045005.

21. Zeng HP, Yang XHO, Wang TT, Yuan GZ, Zhang GH et al. Synthesis, crystal structure, and prediction of hole mobilities of 2,7'-ethylenebis(8-hydroxyquinoline). Crystal Growth and Design 2006; 6: 1697-1702.

22. Barberis VP, Mikroyannidis JA. Synthesis and optical properties of aluminum and zinc quinolates through styryl substituent in 2-position. Synthetic Metals 2006; 156: 865-871.

23. Podeszwa B, Niedbala H, Polanski J, Musiol R, Tabak D et al. Investigating the antiproliferative activity of quinoline-5,8-diones and styrylquinolinecarboxylic acids on tumor cell lines. Bioorganic and Medicinal Chemistry Letters 2007; 17: 6138-6141.

24. Musiol R, Jampilek J, Buchta V, Silva L, Nied-Bala H et al. Antifungal properties of new series of quinoline derivatives. Bioorganic and Medicinal Chemistry 2006; 14: 3592-3598.

25. Huang FC, Galemmo RA, Campbell HF. Quinolinyl-benzopyran derivatives as antagonists of leukotriene. US Patent no. 4918081, 1990.

26. Budyka MF, Potashova NI, Gavrishova TN, Li VM. Reconfigurable molecular logic gate operating in polymer film. Journal of Materials Chemistry 2009; 19: 7721-7724.

27. Andryukhina EN, Mashura MM, Fedorova OA, Kuzmina LG, Khovard DAK et al. Synthesis and structures of azine-based crown-containing hetarylphenylethenes. Russian Chemical Bulletin 2005; 54: 1700-1709.

28. Varbanova SJ, Chervenkov SK. Synthesis of new alkoxy-hydroxystyryl-2-quinoline and alkoxy-hydroxystyryl-2-quinoline based and of their hydrochloride with expected biological action. Dokladi Na Bolgarskata Akademiya Na Naukite 1986; 39: 69-72.

29. Kaslow CE, Stayner RD. Ozonolysis of styryl derivatives of nitrogen heterocycles. Journal of the American Chemical Society 1945; 67: 1716-1717.

30. Yaragorla S, Singh G. C(sp3)–H functionalization of methyl azaarenes: a calcium-catalyzed facile synthesis of (E)-2-styryl azaarenes and 2-aryl-1,3-bisazaarenes. Tetrahedron Letters 2015; 56: 5924-5929.

31. Che CM, Kwok CC, Lai SW, Rausch AF, Finkenzeller WJ et al. Photophysical properties and OLED applications of phosphorescent platinum(II) Schiff base complexes. Chemistry - A European Journal 2010; 16: 233-247.

32. Gülseven Sıdır Y, Sıdır İ, Berber H, Türkoğlu G. Solvatochromic behavior and electronic structure of some symmetric 2-aminophenol Schiff base derivatives. Journal of Molecular Liquids 2014; 199: 57-66.

33. Sıdır İ, Gülseven Sıdır Y, Berber H, Demiray F. Emerging ground and excited state dipole moments and external electric field effect on electronic structure. A solvatochromism and theoretical study on 2-((phenylimino)methyl)phenol derivatives. Journal of Molecular Liquids 2015; 206: 56-67.

34. Mao F, Yan J, Li J, Jia X, Miao H et al. New multi-target-directed small molecules against Alzheimer's disease: a combination of resveratrol and clioquinol. Organic and Biomolecular Chemistry 2014; 12: 5936-5944.

35. Bilot L, Kawski A. Zur Theorie des Einflusses von Lösungsmitteln auf die Elektronenspektren der Moleküle. Zeitschrift für Naturforschung A 1962; 17: 621-627.

36. Kawski A. Zur Lösungsmittelabhängigkeit der Wellenzahl von Elektronenbanden Lumineszierender Moleküle und über die Bestimmung der Elektrischen Dipolmomente im Anregungszustand. Acta Physica Polonica 1966; 29: 507-518.

37. Kawski A. Progress in Photochemistry and Photophysics. Boca Raton, FL, USA: CRC Press, 1992.

38. Kawski A. On the estimation of excited-state dipole moments from solvatochromic shifts of absorption and fluorescence spectra. Zeitschrift für Naturforschung A 2002; 57: 255-262.

39. Kawski A. Über die Anomale Stokessche Rotverschiebung der Absorptions- und Fluoreszenzmaxima von 4-Aminophthalimid in Mischungen aus Dioxan und Wasser. Acta Physica Polonica 1964; 25: 285-290.

40. Kawski A. Bojarski P, Kuklinski B, Estimation of ground- and excited-state dipole moments of Nile Red dye from solvatochromic effect on absorption and fluorescence spectra. Chemical Physics Letters 2008; 463: 410-412.

41. Kawski A. Solvent-shift effect on electronic spectra and excited-state diople moments. In: Rabek JF (editor). Progress in Photochemistry and Photophysics vol. 5. Boca Raton, FL, USA: CRC Press, 1992; pp. 1-48.

42. Lippert E. Dipolmoment und Elektronenstruktur von angeregten Molekülen. Zeitschrift für Naturforschung A 1955; 10: 541-545.

43. Mataga N, Kaifu Y, Koizumi M. Solvent effects upon fluorescence spectra and the dipole moments of excited molecules. Bulletin of the Chemical Society Japan 1956; 29: 465-470.

44. Bakhshiev NG. Universal intermolecular interactions and their effect on the position of the electronic spectra of molecules in two component solutions. Optical Spectroscopy 1964; 16: 821-832.

45. Chamma A, Viallet P. Determination du moment dipolaire d'une molcule dans un tat excit singule. Comptes rendus de l'Académie des Sciences 1970; 270: 1901-1904.

46. Reichardt C. Dyes as solvent polarity indicators. Chemical Reviews 1994; 94: 2319-2358.

47. Reichardt C. Solvents and Solvent Effects in Organic Chemistry. Third ed. Weinheim, Germany: Wiley-VCH, 2005.

48. Lide DR (editor). CRC Handbook of Chemistry and Physics, 76th ed. Boca Raton, FL, USA: CRC Press, 1995.

49. Kamlet MJ, Abboud JL, Abraham MH, Taft RW. A comprehensive collection of the solvatochromic parameters, .pi.*, .alpha., and .beta., and some methods for simplifying the generalized solvatochromic equation. Journal of Organic Chemistry 1983; 48: 2877-2887.

50. Kamlet MJ, Abboud JL, Taft RW. The π^* scale of solvent polarities. Journal of the American Chemical Society 1997; 99: 6027-6038.

51. Catalán J. Toward a generalized treatment of the solvent effect based on four empirical scales: dipolarity (SdP, a new scale), polarizability (SP), acidity (SA), and basicity (SB) of the medium. Journal of Physical Chemistry B 2009; 113: 5951-5960.

52. Kohn W, Sham LJ. Self-consistent equations including exchange and correlation effects. Physical Reviews 1965; 140: 1133-1138.

53. Frisch MJ, Trucks GW, Schlegel HB, Scuseria GE, Robb MA et al. Gaussian 09, Revision D.01. Wallingford CT, USA: Gaussian, Inc., 2013.

54. Becke AD. Density-functional exchange-energy approximation with correct asymptotic behavior. Physical Reviews A 1988; 38: 3098-3100.

55. Lee C, Yang W, Parr RG. Development of the Colle–Salvetti correlation energy formula into a functional of the electron density. Physical Reviews B 1988; 37: 785-789.

56. Lan SC, Liu YH. TDDFT study on the excited-state proton transfer of 8-hydroxyqinoline: key role of the excited-state hydrogen-bond strengthening. Spectrochimica Acta Part A 2015; 139: 49-53.

57. Sun YX, Hao QL, Wei WX, Yu ZX, Lu LD et al. Experimental and density functional studies on 4-(3,4-dihydroxybenzylideneamino)antipyrine, and 4-(2,3,4-trihydroxybenzylideneamino)antipyrine. Journal of Molecular Structure: Theochem 2009; 904: 74-82.

58. Andraud C, Brotin T, Garcia C, Pelle F, Goldner P et al. Theoretical and experimental investigations of the nonlinear optical properties of vanillin, polyenovanillin, and bisvanillin derivatives. Journal of the American Chemical Society 1994; 116: 2094-2102.

59. Geskin VM, Lambert C, Bredas JL. Origin of high second- and third-order nonlinear optical response in ammonio/borato diphenylpolyene zwitterions:? the remarkable role of polarized aromatic groups. Journal of the American Chemical Society 2003; 125: 15651-15658.

60. Nakano M, Fujita H, Takahata M, Yamaguchi K. Theoretical study on second hyperpolarizabilities of phenylacetylene dendrimer:? toward an understanding of structure–property relation in NLO responses of fractal antenna dendrimers. Journal of the American Chemical Society 2002; 124: 9648-9655.

61. Sajan D, Joe H, Jayakumar VS, Zaleski J. Structural and electronic contributions to hyperpolarizability in methyl p-hydroxy benzoate. Journal of Molecular Structure 2006; 785: 43-53.

62. Zhang R, Du B, Sun G, Sun YX. Experimental and theoretical studies on o-, m- and p-chlorobenzylideneaminoantipyrines. Spectrochimica Acta Part A 2010; 75: 1115-1124.

63. Kleinman DA. Nonlinear dielectric polarization in optical media. Physical Reviews 1962; 126: 1977-1979.

64. Thanthiriwatte KS, Nalin de Silva KM. Non-linear optical properties of novel fluorenyl derivatives—ab initio quantum chemical calculations. Journal of Molecular Structure: Theochem 2002; 617: 169-175.

65. Tanak H, Pawlus K, Marchewka MK, Pietraszko A. Structural, vibrational and theoretical studies of anilinium trichloroacetate: new hydrogen bonded molecular crystal with nonlinear optical properties. Spectrochimica Acta Part A: Molecular and Biomolecular Spectroscopy 2014; 118: 82-93.

66. Tanak H, Agar AA, Buyukgungor O. Experimental (XRD, FT-IR and UV–Vis) and theoretical modeling studies of Schiff base (E)-N′-((5-nitrothiophen-2-yl)methylene)-2-phenoxyaniline. Spectrochimica Acta Part A: Molecular and Biomolecular Spectroscopy 2014; 118: 672-682.

67. Tanak H. Molecular structure, spectroscopic (FT-IR and UV-Vis) and DFT quantum-chemical studies on 2-[(2,4-dimethylphenyl)iminomethyl]-6-methylphenol Molecular Physics 2014; 112: 1553-1565.